Non-cooperative detection of weak spread-spectrum signals in AWGN

J.D. Vlok and J.C. Olivier

***Abstract*—A semi-blind method based on principal component analysis (PCA) and sequence synchronisation is proposed to detect direct sequence spread-spectrum (DSSS) signals in a non-cooperative setting under low signal-to-noise ratio (SNR) conditions. The intercepted signal is segmented to form a detection matrix from which a feature is extracted through cyclic shifting. Signal detection is then performed using a test statistic based on this feature. The carrier frequency and sequence duration of the signal to be detected are assumed known. Theoretical analysis and a computer simulation study show that the performance of the new detection method is superior to classic energy detection (ED) in an additive white Gaussian noise (AWGN) channel.**

I. Introduction

Cooperative detection techniques are used in communication systems where the receiver has perfect knowledge of all the parameters used by the transmitter. The receiver then uses detection and estimation of the parameters as necessary to identify the beginning of the transmission (e.g. in asynchronous communication) or to identify inactive channels (e.g. in cognitive radio). However, in non-cooperative applications such as spectrum surveillance and electronic interception, the receiver has no knowledge of the parameters used by the transmitter. Under these conditions blind detection and estimation techniques are used. If the receiver has some information on the parameters available or is able to estimate some of the parameters, semi-blind detection techniques may be used. This paper is concerned with the performance of semi-blind detection techniques, specifically for the detection of weak spread-spectrum signals.

In this paper new results and a new method for the detection of weak unknown deterministic signals in an additive white Gaussian noise (AWGN) channel are presented. The class of signals investigated is direct sequence spread-spectrum (DSSS) where a large transmission bandwidth is employed to hide the signal below the noise level. Several techniques addressing DSSS detection are available in the literature. Energy detection (ED) of spread-spectrum signals is presented in [1]. Techniques based on higher order spectral analysis are presented in [2], and cyclostationary analysis where the autocorrelation of segments of the intercepted signal is used as basis of detection is presented in [3]. Approaches to estimate the spreading sequence from the intercepted signal include signal correlation of synchronised sequences [4], principal component analysis (PCA) [5] and neural network techniques [6].

J.D. Vlok is with Defence, Peace, Safety & Security (DPSS), Council for Scientific and Industrial Research (CSIR), Pretoria, South Africa, 0001. E-mail: jvlok@csir.co.za

J.C. Olivier is with the School of Engineering, University of Tasmania, Hobart, Australia, 7005.

The new method presented in this paper is based on spreading sequence synchronisation [4] and PCA [5] which are used to extract the largest eigenvalue sequence as detection feature from the sample covariance matrix (SCM) of the intercepted signal. Two detection techniques are presented; the first technique uses the eigenvalue sequence directly and the second technique uses the frequency content of the eigenvalue sequence to perform detection. The techniques are semi-blind since certain aspects of the signal to be detected and the noise are assumed known. Signal knowledge assumed known include the carrier frequency and the sequence duration. These two parameters can be estimated using correlation techniques [3], [4] or the detection algorithm can sweep through a certain predefined range of these two parameters in order to search for signal activity. The noise statistics (including the probability density function (PDF) and power level) are assumed known in order to calculate the detection threshold. Noise statistics can be estimated by observing the surveillance band over long periods of time assuming that the signal of interest is not always present.

In this paper the performance of the detection techniques is evaluated and compared using the binary hypothesis testing approach (see [7]) over a range of signal-to-noise ratios (SNRs). Although the detection algorithms do not assume knowledge of the SNR, the detection performance is expressed in terms thereof. This paper compares the performance of the two new techniques with classic ED, assuming the signal of interest is a baseband binary phase shift keying (BPSK) DSSS communication signal. It is shown that the new detection techniques have superior performance to classic ED under AWGN channel conditions.

The paper is organised as follows. Section II considers the target communication system and intercept receiver. Section III describes the new feature extraction technique and Section IV evaluates the performance thereof in an AWGN channel. Section V reviews ED and presents the two new detection techniques. Section VI investigates the computational complexity and Section VII presents simulated detection performance results for each detection technique. The paper is concluded in Section VIII.

II. Communication and detection systems

This section considers the target communication system and the intercept receiver used to detect communication activity originating from the target system in the surveillance band.

A. Target communication system

The target communication system considered in this paper is a BPSK DSSS system employing a Walsh spreading code of

length $N = 64$. In order to establish the required SNR level at which non-cooperative detection must be performed, the error probability achievable by the intended receiver (the receiver of the target communication system for which the communication is intended) should be investigated. The error probability of BPSK in AWGN is well known as [8]

$$P_e = Q\left(\sqrt{\frac{2\epsilon_b}{N_0}}\right) \tag{1}$$

with $Q(\cdot)$ the tail probability of the standard normal distribution, ϵ_b the energy per bit and N_0 the single-sided noise power spectral density. The error probability can be expressed from (1) as

$$P_e = Q\left(\sqrt{N_s\ \mathrm{SNR}}\right) \tag{2}$$

with N_s the number of samples used to represent a single transmitted bit. Although (1) and (2) are equivalent, (2) is preferred in the non-cooperative context since the signal and surveillance bandwidths are not necessarily equal and (2) is required to illustrate the relation between the DSSS processing gain and the SNR advantage obtained by spreading.

If a single sample is used in the receiver to represent one chip of the spreading sequence then $N_s = N$. The bit error probability curves for the unspreaded BPSK case ($N = 1$) and the spreaded case ($N = 64$) are shown in Figure 1. The processing gain $P_G = 10\ \log_{10} N \approx 18$ dB (for $N = 64$) is the SNR advantage obtained by spreading and corresponds to the SNR difference between the two curves for any P_e value in Figure 1. The intended receiver would therefore be able to despread a DSSS signal with $\mathrm{SNR} = -10$ dB (before despreading) to $\mathrm{SNR} = 8$ dB (after despreading) to achieve communications at $P_e \approx 6 \times 10^{-3}$. Assuming the distances between the transmitter and intended receiver and the same transmitter and the intercept receiver are equivalent, the intercept receiver (not knowing the spreading code) is now faced with the challenge of detecting DSSS signal activity using a received signal with $\mathrm{SNR} = -10$ dB. If the intercept receiver is further off in distance, an even lower SNR will result. Powerful detection algorithms are therefore required to enable the intercept receiver to compete with the target communication system and detect DSSS signals at very low SNR levels.

B. Intercept receiver

The detection algorithms presented in this paper are envisaged to be implemented on a system with a receiver architecture similar to the one presented in [9]. The received radio frequency (RF) signal is filtered using a wideband front-end filter, mixed down and then sampled with a high-speed (greater than twice the surveillance bandwidth) analog-to-digital converter. The resultant baseband signal is then analysed without further filtering stages. For this receiver architecture, the signal model presented in [4] can be used to develop the detection algorithms. For simplicity of analysis, perfect timing and carrier synchronisation are assumed such that one sample is used to represent a single chip of the spreading sequence in the intercept receiver. The intercepted discrete DSSS signal can then be expressed as

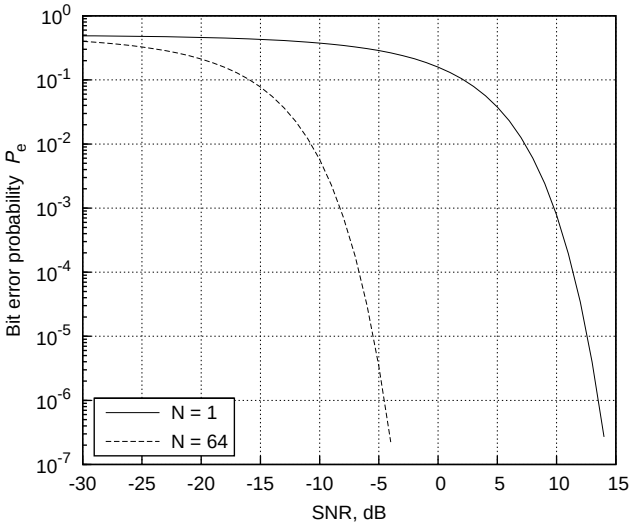

Fig. 1. Bit error probability for unspreaded ($N = 1$) and spreaded ($N = 64$) BPSK DSSS in AWGN.

$$\boldsymbol{y}(nT_c) = \sigma_x \boldsymbol{d}(nT_c)\boldsymbol{c}(nT_c) + \sigma_w \boldsymbol{w}(nT_c) \tag{3}$$

with the chip number $n = 1, 2, \ldots, N$ and T_c the chip interval. $\boldsymbol{c}$ is the length-N ($N >> 1$) pseudo-noise code sequence with period $T_{sym} = NT_c$ and $\boldsymbol{d}$ the data sequence assumed to be invariant over T_{sym}. Since the target communication system is a BPSK DSSS system, both $\boldsymbol{c}$ and $\boldsymbol{d}$ are sequences with values ± 1. The noise sequence is represented by $\boldsymbol{w} \sim \mathcal{N}(\mu = 0, \sigma^2 = 1)$. The code, data and noise sequences are also assumed independent of each other. The constants σ_x and σ_w are included to scale the signal and noise sequences respectively in order to obtain different SNR values, using

$$\mathrm{SNR} = \frac{\sigma_x^2}{\sigma_w^2} \tag{4}$$

which is the SNR before despreading.

Before the detection feature can be extracted from the intercepted signal, some signal formatting is required. The intercepted signal is firstly divided into non-overlapping segments of length equal to N. Secondly, these segments are stacked to form the $N \times N$ detection matrix given by

$$\boldsymbol{Y} = \sigma_x \boldsymbol{X} + \sigma_w \boldsymbol{W} \tag{5}$$

with $\boldsymbol{X}$ the data and $\boldsymbol{W}$ the noise matrices. The detection technique presented in this paper then takes $\boldsymbol{Y}$ as input and decides whether a DSSS signal is present or not.

III. Feature extraction

The detection feature is the largest eigenvalue sequence of the SCM of the intercepted signal stacked in the detection matrix $\boldsymbol{Y}$. The feature is extracted by performing PCA on $\boldsymbol{Y}$ while cyclically shifting the matrix. This section considers the noise-free scenario with $\sigma_x > 0$ and $\sigma_w = 0$ such that $\boldsymbol{Y} = \sigma_x \boldsymbol{X}$. The scenario with $\sigma_w > 0$ is considered in Section IV. Although this section considers real binary data and spreading

sequences, the result can easily be extended to the complex case.

A. Constructing the data matrix

The spreading sequence $\boldsymbol{c} = [c_1, c_2, \ldots, c_N]$ containing N chips is used to spread the data sequence $\boldsymbol{d} = [d_1, d_2, \ldots, d_N]$ containing N bits. If the receiver started intercepting at the beginning of a new sequence, the data matrix can be denoted as

$$\boldsymbol{X}_0 = \begin{bmatrix} d_1c_1 & d_1c_2 & \ldots & d_1c_{N-1} & d_1c_N \\ d_2c_1 & d_2c_2 & \ldots & d_2c_{N-1} & d_2c_N \\ \vdots & \vdots & \ddots & \vdots & \vdots \\ d_{N-1}c_1 & d_{N-1}c_2 & \ldots & d_{N-1}c_{N-1} & d_{N-1}c_N \\ d_Nc_1 & d_Nc_2 & \ldots & d_Nc_{N-1} & d_Nc_N \end{bmatrix} \tag{6}$$

which will be referred to as the aligned data matrix since the code sequence elements are aligned to the columns of $\boldsymbol{X}_0$; i.e. c_1 is in column 1, c_2 in column 2, and so on.

B. Principal component analysis

To perform PCA on the aligned data matrix, the covariance matrix of $\boldsymbol{X}_0$ is computed and then eigen decomposition is performed. The $N \times N$ covariance matrix is defined as (see [10]–[12])

$$\mathbf{COV}(\boldsymbol{X}_0) = E\left[\boldsymbol{X}_0^T\boldsymbol{X}_0\right] \tag{7}$$

with $[\cdot]^T$ the matrix transpose. The covariance matrix can be estimated using the SCM

$$\boldsymbol{R}(\boldsymbol{X}_0) = \frac{1}{N}\sum_{n=1}^{N}\boldsymbol{x}_n^T\boldsymbol{x}_n = \frac{1}{N}\boldsymbol{X}_0^T\boldsymbol{X}_0 \tag{8}$$

with $\boldsymbol{x}_n$ the n^{th} row of $\boldsymbol{X}_0$. The SCM of the aligned data matrix can therefore be expressed as

$$\boldsymbol{R}(\boldsymbol{X}_0) = \left[\frac{1}{N}\sum_{n=1}^{N}d_n^2\right]\boldsymbol{c}^T\boldsymbol{c} = \boldsymbol{c}^T\boldsymbol{c} \tag{9}$$

which is a positive-semidefinite (and by definition symmetric) matrix [13]. The simplification in (9) follows from the fact that $d_n^2 = 1$ for all values of n. By performing elementary row operations on $\boldsymbol{R}(\boldsymbol{X}_0)$ it can be shown that the row echelon form $\boldsymbol{R}_{\text{ech}}(\boldsymbol{X}_0)$ is an $N \times N$ matrix with only the first row being nonzero. $\boldsymbol{R}(\boldsymbol{X}_0)$ therefore has a rank of one and thus only one nonzero eigenvalue [7]. This can be expected since $\boldsymbol{X}_0$ has N linearly dependent rows. The nonzero eigenvalue of $\boldsymbol{R}(\sigma_x\boldsymbol{X}_0)$ can therefore be expressed as

$$\begin{aligned} \lambda_{X,1} &= \text{tr}(\boldsymbol{R}(\sigma_x\boldsymbol{X}_0)) \\ &= \sigma_x^2\left[\sum_{n=1}^{N}c_n^2\right] \\ &= \sigma_x^2 N \end{aligned} \tag{10}$$

since the trace of a matrix equals the sum of its eigenvalues [13] and $c_n^2 = 1$. Furthermore, $\lambda_{X,1}$ is nonnegative and real, since the eigenvalues of positive-semidefinite matrices are nonnegative and real [7].

C. Cyclic shifting

Shifting is performed by discarding the first received sample and appending a new sample at the end of the sample sequence. The data matrix $\boldsymbol{X}_0$ after $k \in [0, N)$ shifts can then be written as

$$\boldsymbol{X}_k = \begin{bmatrix} d_1c_{k+1} & \ldots & d_1c_N & d_2c_1 & \ldots & d_2c_k \\ d_2c_{k+1} & \ldots & d_2c_N & d_3c_1 & \ldots & d_3c_k \\ \vdots & \ddots & \vdots & \vdots & \ddots & \vdots \\ d_{N-1}c_{k+1} & \ldots & d_{N-1}c_N & d_Nc_1 & \ldots & d_Nc_k \\ d_Nc_{k+1} & \ldots & d_Nc_N & d_{N+1}c_1 & \ldots & d_{N+1}c_k \end{bmatrix} \tag{11}$$

$\boldsymbol{X}_k$ for $k \geq N$ can be obtained in a similar way by noting that $\boldsymbol{X}_k$ will be in aligned form for any nonnegative multiple of N shifts starting from $\boldsymbol{X}_0$. $\boldsymbol{X}_N$ will therefore have the same form as $\boldsymbol{X}_0$ though the contents of the entire matrix are shifted up one row with the top row removed and the bottom row replaced by a new sequence. The effect of a single sample shift on the data matrix is a cyclic left shift of all the columns followed by a cyclic upwards shift of the last column and finally replacing the bottom right element with the new sample. The resultant effect on the SCM is a shift diagonally upwards (in a North West direction) such that the first row and column are removed and the last row and column are replaced by new values due to the new data sample in the last row and column position of the data matrix. The SCM of $\boldsymbol{X}_k, k \in [0, N)$ can be given as

$$\boldsymbol{R}(\boldsymbol{X}_k) = \boldsymbol{A}_k \circ \left[\boldsymbol{c}_k^T\boldsymbol{c}_k\right] \tag{12}$$

where $\circ$ denotes the Hadamard product operator. $\boldsymbol{c}_k$ is the spreading code $\boldsymbol{c}$ cyclically left-shifted k times given as

$$\boldsymbol{c}_k = [c_{k+1}, c_{k+2}, \ldots c_N, c_1, \ldots c_k] \tag{13}$$

such that the first $N_k = N - k$ elements in $\boldsymbol{c}_k$ correspond to the last N_k elements in $\boldsymbol{c}$. $\boldsymbol{A}_k$ is an $N \times N$ coefficient matrix

$$\boldsymbol{A}_k = \begin{bmatrix} \alpha_{11}\boldsymbol{J}_{N_k,N_k} & \alpha_{12}\boldsymbol{J}_{N_k,k} \\ \alpha_{12}\boldsymbol{J}_{k,N_k} & \alpha_{22}\boldsymbol{J}_{k,k} \end{bmatrix} \tag{14}$$

consisting of four submatrices where $\boldsymbol{J}_{m,n}$ denotes the $m \times n$ matrix of ones. The coefficient values are

$$\begin{aligned} \alpha_{11} &= \frac{1}{N}\sum_{n=1}^{N}d_n^2 = 1 \\ \alpha_{12} &= \frac{1}{N}\sum_{n=1}^{N}d_nd_{n+1} \\ \alpha_{22} &= \frac{1}{N}\sum_{n=2}^{N+1}d_n^2 = 1 \end{aligned}$$

since $d_n^2 = 1$. The form of the coefficient matrix $\boldsymbol{A}_k$ arises from the fact that the first N_k columns of each row of $\boldsymbol{X}_k$ have the same data bit value as the corresponding row of $\boldsymbol{X}_0$. The last k columns of each row of $\boldsymbol{X}_k$ contain the data bit that overflowed from the row beneath (e.g. the last k columns of the first row of $\boldsymbol{X}_k$ contain d_2).

By performing elementary row operations on $\boldsymbol{R}(\boldsymbol{X}_k)$ it can be shown that the row echelon form $\boldsymbol{R}_{\text{ech}}(\boldsymbol{X}_k)$ is an $N \times N$ matrix

with only the first two rows being nonzero (except when the data matrix is aligned - only the first row is then nonzero). The second row of $\boldsymbol{R}_{\text{ech}}(\boldsymbol{X}_k)$ contains N_k zeros followed by k nonzero elements and therefore $\boldsymbol{R}_{\text{ech}}(\boldsymbol{X}_k)$ contains a maximum of only two nonzero rows for all values of k. $\boldsymbol{R}(\boldsymbol{X}_k)$ therefore contains a maximum of two nonzero (also nonnegative real) eigenvalues and the data matrix $\boldsymbol{X}_k$ consequently has a maximum of only two principal components.

D. Largest eigenvalues

Since $\boldsymbol{R}(\sigma_x\boldsymbol{X}_k)$ has a maximum of only two nonzero eigenvalues, its trace can be expressed in terms of the eigenvalues as

$$\text{tr}(\boldsymbol{R}(\sigma_x\boldsymbol{X}_k)) = \sum_{p=1}^{2}\lambda_{X,p} = \lambda_{X,1} + \lambda_{X,2} \tag{15}$$

with the largest eigenvalue $\lambda_{X,1} \geq \lambda_{X,2}$. Note that $\lambda_{X,p}$ depends on the shift parameter k but this dependence is omitted for the sake of simplifying notation. Using (12)-(14) the trace can be expressed in terms of the matrix elements as

$$\begin{aligned}\text{tr}\left(\boldsymbol{R}(\sigma_x\boldsymbol{X}_k)\right) &= \sigma_x^2\sum_{n=1}^{N}\left[\boldsymbol{R}(\boldsymbol{X}_k)\right]_{nn}\\ &= \sigma_x^2\left(\alpha_{11}\sum_{n=1}^{N_k}\left[\boldsymbol{c}_k^T\boldsymbol{c}_k\right]_{nn} + \alpha_{22}\sum_{n=N_k+1}^{N}\left[\boldsymbol{c}_k^T\boldsymbol{c}_k\right]_{nn}\right)\\ &= \sigma_x^2 N\end{aligned} \tag{16}$$

with $[\cdot]_{nn}$ denoting the diagonal entries of each matrix. The simplification in (16) follows from the fact that $\alpha_{11} = \alpha_{22} = 1$ and $c_n^2 = 1$. The sum of the eigenvalues therefore has a constant value irrespective of the value of k, assuming the signal power σ_x^2 remains constant. (15) can thus be stated as

$$\text{tr}(\boldsymbol{R}(\sigma_x\boldsymbol{X}_k)) = \lambda_{X,1} + \lambda_{X,2} = \sigma_x^2 N \quad \forall\ k. \tag{17}$$

Whenever $\boldsymbol{X}_k$ is aligned, $\lambda_{X,1} = \sigma_x^2 N$ as in (10) and $\lambda_{X,2} = 0$. $\lambda_{X,1}$ therefore exhibits a pattern with period N as $\boldsymbol{X}_k$ is cyclically shifted, since $\lambda_{X,1} \geq \lambda_{X,2}$ for all values of k. $\lambda_{X,1}$ therefore reaches its maximum value $\sigma_x^2 N$ once during every complete cycle of shifting.

1) Eigenvalue bounds: Though it is possible to develop analytic expressions for $\lambda_{X,p}$, such equations would not be tractable since they are functions of all the elements of $\boldsymbol{c}$ and $\boldsymbol{d}$. Instead, in order to describe the behaviour of the largest eigenvalue, bounds on its variation are provided in this section. Since $\boldsymbol{R}(\boldsymbol{X}_k)$ has a maximum rank of two, its eigenvalues are the roots of a quadratic polynomial. By evaluating the eigenvalues of $\boldsymbol{R}(\sigma_x\boldsymbol{X}_k)$ with $d_n^2 = c_n^2 = 1$, it can be shown that the two nonzero eigenvalues can be expressed in the form

$$\lambda_X = \frac{N^2 \pm \sqrt{\Delta}}{2N}\sigma_x^2 \tag{18}$$

with the discriminant of the quadratic polynomial $\Delta \in [0, N^4]$. From (18) the largest eigenvalue of $\boldsymbol{R}(\sigma_x\boldsymbol{X}_k)$ is bounded according to

$$\frac{N\sigma_x^2}{2} \leq \lambda_{X,1} \leq N\sigma_x^2 \tag{19}$$

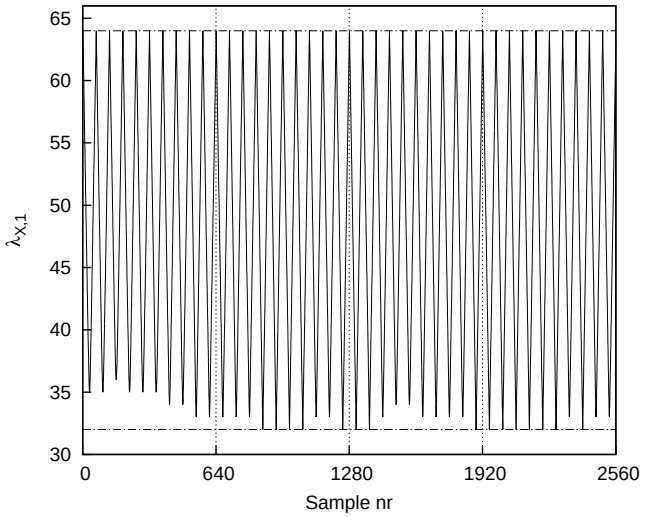

Fig. 2. Example temporal representation of $\lambda_{X,1}$ for $\sigma_x^2 = 1$ and $N = 64$.

Figure 2 shows an example of the temporal variation of $\lambda_{X,1}$ when BPSK data is spread using the Walsh $N = 64$ code with $\sigma_x^2 = 1$. The bounds in Figure 2 are given in (19). Note that the minimum bound for $\lambda_{X,1}$ is not necessarily reached during every cycle; the actual minimum value depends on the input data bits. From (17) the maximum bound for $\lambda_{X,1}$ is however reached during every cycle irrespective of the input data bit values.

IV. Analysis in noise

This section considers the effect of noise on the feature extraction technique. The detection matrix can be written as

$$\boldsymbol{Y}_k = \sigma_x\boldsymbol{X}_k + \sigma_w\boldsymbol{W}_k \tag{20}$$

with the noise matrix in a similar form to $\boldsymbol{X}_k$ given by

$$\boldsymbol{W}_k = \begin{bmatrix} w_{1,k+1} & \cdots & w_{1,N} & w_{2,1} & \cdots & w_{2,k} \\ w_{2,k+1} & \cdots & w_{2,N} & w_{3,1} & \cdots & w_{3,k} \\ \vdots & \ddots & \vdots & \vdots & \ddots & \vdots \\ w_{N-1,k+1} & \cdots & w_{N-1,N} & w_{N,1} & \cdots & w_{N,k} \\ w_{N,k+1} & \cdots & w_{N,N} & w_{N+1,1} & \cdots & w_{N+1,k} \end{bmatrix} \tag{21}$$

containing real independent and identically distributed (i.i.d.) zero mean unity variance Gaussian samples.

A. Noise-only scenario

If $\sigma_x = 0$, the intercepted signal will contain only noise. For any cyclic shift performed on $\boldsymbol{W}_k$, the SCM $\boldsymbol{R}(\sigma_w\boldsymbol{W}_k)$ is a Wishart matrix. The normalised largest eigenvalue of a Wishart matrix is distributed according to the Tracy-Widom law [11], which can be approximated using the Gamma distribution [12], [14]. The distribution of the largest eigenvalue $\lambda_{W,1}$ of $\boldsymbol{R}(\sigma_w\boldsymbol{W}_k)$ can therefore be approximated using the Gamma PDF [12]

$$\gamma(x) = \frac{(x-x_0)^{\alpha-1}}{\theta^\alpha\Gamma(\alpha)}\ \exp\left[\frac{-(x-x_0)}{\theta}\right] \tag{22}$$

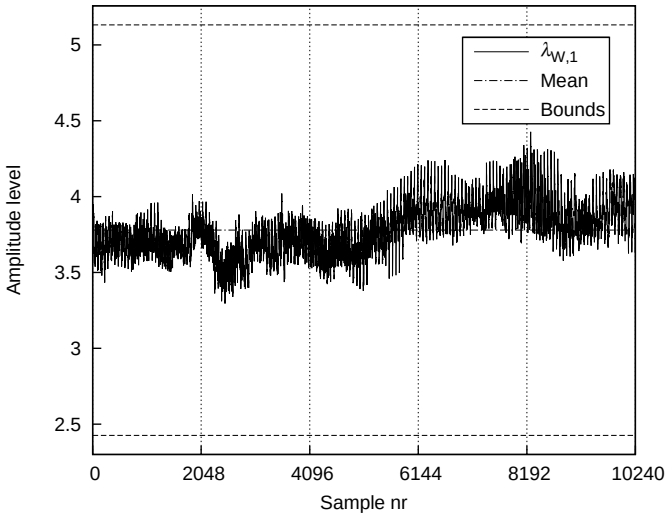

Fig. 3. Example temporal representation of $\lambda_{W,1}$ for $\sigma_w^2 = 1$ and $N = 64$.

with support region $[x_0, x_0 + 2\alpha\theta]$. The parameter values of (22) for $\boldsymbol{W}_k$ with real elements are

$$\begin{aligned} \alpha &= 46.5651 \\ \theta &= 0.1850\ \sigma_w^2\ \sigma_N/N \\ x_0 &= \sigma_w^2\left(\mu_N - 9.8209\sigma_N\right)/N \end{aligned}$$

with the center and scaling parameters

$$\begin{aligned} \mu_N &= \left(\sqrt{N-1}+\sqrt{N}\right)^2 \\ \sigma_N &= \sqrt{\mu_N}\left(\frac{1}{\sqrt{N-1}}+\frac{1}{\sqrt{N}}\right)^{\frac{1}{3}}. \end{aligned}$$

Although $\boldsymbol{R}(\sigma_w\boldsymbol{W}_k)$ is always a Wishart matrix, all SCMs of $\boldsymbol{W}_k$ for shifts from k to $k+N-1$ (starting from any value of k) will contain some identical elements, though not in identical positions. This is due to the diagonal shift on the SCM as explained in Section III-C. It can therefore be expected that a pattern with period N will arise in the eigenvalue sequence of the SCM as the noise matrix is cyclically shifted.

Figure 3 shows an illustration of the temporal variation of $\lambda_{W,1}$ as $\boldsymbol{W}_k$ is cyclically shifted for $\sigma_w^2 = 1$ and $N = 64$. The bounds of $\lambda_{W,1}$ afforded by the support region

$$x_0 \le \lambda_{W,1} \le x_0 + 2\alpha\theta \tag{23}$$

and the measured mean value of $\lambda_{W,1}$ are also shown in Figure 3. It can be shown that the PDF of $\lambda_{W,1}$ illustrated in Figure 3 is accurately predicted by the Gamma approximation of (22) (see [12]).

B. Signal and noise scenario

The SCM of $\boldsymbol{Y}_k$ can be expressed as

$$\begin{aligned} \boldsymbol{R}(\boldsymbol{Y}_k) &= \boldsymbol{R}\left(\sigma_x\boldsymbol{X}_k + \sigma_w\boldsymbol{W}_k\right) \\ &= \sigma_x^2\boldsymbol{R}(\boldsymbol{X}_k) + \sigma_w^2\boldsymbol{R}(\boldsymbol{W}_k) + \boldsymbol{E}_k \end{aligned} \tag{24}$$

with the error matrix expressed as

$$\boldsymbol{E}_k = \frac{\sigma_x\sigma_w}{N}\left[\boldsymbol{X}_k^T\boldsymbol{W}_k + \boldsymbol{W}_k^T\boldsymbol{X}_k\right]. \tag{25}$$

This section considers bounds on the largest eigenvalue $\lambda_{Y,1}$ of $\boldsymbol{R}(\boldsymbol{Y}_k)$ using the Weyl inequalities [15]–[17]. Although it is often assumed that $\boldsymbol{E}_k = \boldsymbol{0}$ (see for example [15]), the effect of the error matrix is also considered here.

1) Weyl inequalities: The eigenvalue spectrum of the sum of two $N \times N$ Hermitian (or real symmetric) matrices $\boldsymbol{A}$ and $\boldsymbol{B}$ can be described using the Weyl inequalities. Arranging all eigenvalues in decreasing order ($\lambda_1 \ge \cdots \ge \lambda_N$) the p^{th} largest eigenvalue of the matrix sum $\boldsymbol{A}+\boldsymbol{B}$ is bounded according to

$$L_p \le \lambda_p(\boldsymbol{A}+\boldsymbol{B}) \le U_p \tag{26}$$

with the upper and lower bounds respectively given by [18]

$$U_p = \min\{\lambda_i(\boldsymbol{A}) + \lambda_j(\boldsymbol{B}) \ :\ i+j = p+1\} \tag{27}$$

$$L_p = \max\{\lambda_i(\boldsymbol{A}) + \lambda_j(\boldsymbol{B}) \ :\ i+j = p+N\} \tag{28}$$

with the eigenvalue index values $i, j \in [1, N]$. Note that any eigenvalue sum combination in (27) and (28) is respectively a valid upper and lower bound. Taking the minimum in (27) and the maximum in (28) will however result in the tightest bounds. The upper bound for the largest eigenvalue ($p = 1$) can be obtained from (27) as

$$U_1 = \lambda_1(\boldsymbol{A}) + \lambda_1(\boldsymbol{B}) \tag{29}$$

since there is only one solution ($i = j = 1$) to the index equation $i+j = 2$. The lower bound for $p = 1$ can be obtained from (28) as

$$\begin{aligned} L_1 = \max\{&[\lambda_1(\boldsymbol{A}) + \lambda_N(\boldsymbol{B})], [\lambda_2(\boldsymbol{A}) + \lambda_{N-1}(\boldsymbol{B})], \ldots \\ &\ldots, [\lambda_N(\boldsymbol{A}) + \lambda_1(\boldsymbol{B})]\} \end{aligned} \tag{30}$$

since $i+j = 1+N$. In order to use the Weyl inequalities, it can easily be verified mathematically that the matrices $\sigma_x^2\boldsymbol{R}(\boldsymbol{X}_k)$, $\sigma_w^2\boldsymbol{R}(\boldsymbol{W}_k)$, $\sigma_x^2\boldsymbol{R}(\boldsymbol{X}_k) + \sigma_w^2\boldsymbol{R}(\boldsymbol{W}_k)$ and $\boldsymbol{E}_k$ are all symmetric.

2) Eigenvalue bounds of $\mathbf{E}_k$*:* When N is small or correlation exists between the signal and noise sequences, the error matrix $\boldsymbol{E}_k$ given in (25) cannot be neglected in (24). This section considers the upper and lower limits, respectively, of the largest eigenvalue $\lambda_{E,1}$ and the smallest eigenvalue $\lambda_{E,N}$ of $\boldsymbol{E}_k$ in order to derive bounds for $\lambda_{Y,1}$. Each element of $\boldsymbol{X}_k$ in (11) equals ± 1 and each element of $\boldsymbol{W}_k$ given in (21) is independently drawn from $\mathcal{N}(0,1)$. Each element of $\boldsymbol{X}_k^T\boldsymbol{W}_k$ (and $\boldsymbol{W}_k^T\boldsymbol{X}_k$) is therefore the sum of N random variables drawn independently from $\mathcal{N}(0,1)$ such that each element is distributed according to $\mathcal{N}(0,N)$. The sum $\boldsymbol{X}_k^T\boldsymbol{W}_k + \boldsymbol{W}_k^T\boldsymbol{X}_k$ will therefore result in a matrix with main diagonal elements distributed according to $\mathcal{N}(0,4N)$ and all other elements distributed according to $\mathcal{N}(0,2N)$. Since $\boldsymbol{E}_k$ is a real symmetric matrix with all entries symmetrically distributed around 0, the eigenvalue limits can be given as [19]

$$\lambda(\boldsymbol{E}_k) \in [-Nb, Nb] \tag{31}$$

with the entries of $\boldsymbol{E}_k$ in the range $[-b, b]$. Since the elements of $\boldsymbol{E}_k$ are normally distributed and [19] requires a fixed range, the support region of the matrix entries should be truncated. The loss in tail probability mass of $\mathcal{N}(0,\sigma^2)$ due to truncation can be described in terms of the Q-function [8] as

$$Q\left(\frac{b}{\sigma}\right) = Q(\beta) \tag{32}$$

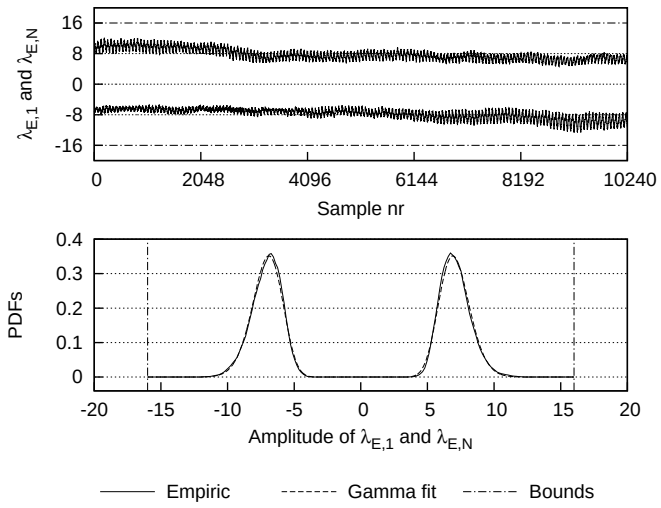

Fig. 4. Largest and smallest eigenvalues of $\boldsymbol{E}_k$ and the corresponding PDF of each for $\sigma_x^2 = \sigma_w^2 = 1$ and $N = 64$.

with

$$b = \beta\sigma\{(\boldsymbol{E}_k)_{ij}\} \tag{33}$$

where β is the factor of the standard deviation at which $\mathcal{N}(0, \sigma^2)$ is truncated. The standard deviation in (33) is denoted by $\sigma\{(\boldsymbol{E}_k)_{ij}\}$ with $i = j$ for the diagonal entries and $i \neq j$ for the off-diagonal entries. Although all entries of $\boldsymbol{E}_k$ are confined to the interval of the diagonal entries ($(\boldsymbol{E}_k)_{jj}$ has twice the variance of $(\boldsymbol{E}_k)_{ij}$), using $i = j$ in (33) will result in very conservative bounds. It can be shown that the lower and upper bounds in (31) would only be attained if all entries of $\boldsymbol{E}_k$ were, respectively, $-b$ and b (see [20]). The standard deviation of the majority of the matrix elements (i.e. the off-diagonal entries) is often used to calculate eigenvalue bounds (see for example [21], [22] for the case where all matrix elements are i.i.d.). Using (25) and the standard deviation of the off-diagonal entries in (33), the eigenvalue bounds of $\boldsymbol{E}_k$ can therefore be expressed using (31) with

$$Nb = \beta\sigma_x\sigma_w\sqrt{2N}. \tag{34}$$

The tightness of the bounds further depends on the value of the factor β in (34). Empirical results indicate that choosing $\beta = \sqrt{2}$ results in valid bounds such that

$$\lambda(\boldsymbol{E}_k) \in [-2\sigma_x\sigma_w\sqrt{N}, 2\sigma_x\sigma_w\sqrt{N}]. \tag{35}$$

Simulated sequences of the largest and smallest eigenvalues of $\boldsymbol{E}_k$ for $\sigma_x^2 = \sigma_w^2 = 1$ and $N = 64$ and the bounds of (35) are shown in Figure 4. The PDF of each sequence is also shown in the figure; $\lambda_{E,1}$ seems to have a Gamma PDF and the two PDFs are mirror images.

3) Bounds of $\lambda_{Y,1}$ when $\mathbf{E}_k = \mathbf{0}$: This section considers the bounds of the largest eigenvalue of $\boldsymbol{R}(\boldsymbol{Y}_k)$ for the scenario where the data and noise are uncorrelated (when N is large) such that (24) can be written as

$$\boldsymbol{R}(\boldsymbol{Y}_k) = \sigma_x^2\boldsymbol{R}(\boldsymbol{X}_k) + \sigma_w^2\boldsymbol{R}(\boldsymbol{W}_k). \tag{36}$$

The eigenvalue bounds of $\boldsymbol{R}(\boldsymbol{Y}_k)$ can be expressed using (26) to (28) with $\boldsymbol{A} = \sigma_x^2\boldsymbol{R}(\boldsymbol{X}_k)$ and $\boldsymbol{B} = \sigma_w^2\boldsymbol{R}(\boldsymbol{W}_k)$. According to (29) the upper bound U_1 of $\lambda_{Y,1}$ is

$$\begin{aligned} U_1 &= \lambda_{X,1} + \lambda_{W,1} \\ &= N\sigma_x^2 + x_0 + 2\alpha\theta \end{aligned} \tag{37}$$

obtained by summing the upper bounds of (19) and (23). According to (30) the lower bound L_1 can be expressed as

$$\begin{aligned} L_1 &= \max\{[\lambda_{X,1} + \lambda_{W,N}], [\lambda_{X,2} + \lambda_{W,N-1}], \\ &\quad [\lambda_{W,N-2}], \ldots, [\lambda_{W,1}]\} \\ &= \max\{\lambda_{X,1}, \lambda_{W,1}\} \end{aligned} \tag{38}$$

using the fact that $\lambda_{X,i} = 0$ for $i > 2$, since $\boldsymbol{R}(\sigma_x\boldsymbol{X}_k)$ has a maximum of only two nonzero eigenvalues (see Section III-D) and the fact that the smallest eigenvalue $\lambda_{W,N}$ approaches zero (even for small values of N [15], [23]) since the detection matrix is square (From [23] the asymptotic lower bound of the eigenvalue spectrum of the SCM of an $M \times N$ noise matrix is $b_- = \left(1 - \sqrt{N/M}\right)^2$. In the case considered here $N = M$, such that $b_- = 0$.). By substituting the lower bounds of (19) and (23) into (38), the lower bound can be expressed as

$$L_1 = \max\left\{\frac{N\sigma_x^2}{2}, x_0\right\} \tag{39}$$

with $N\sigma_x^2/2 > x_0$ if $\text{SNR} > 2(\mu_N - 9.8209\sigma_N)/N^2$ using the value of x_0 from Section IV-A.

4) Bounds of $\lambda_{Y,1}$ when $\mathbf{E}_k \neq \mathbf{0}$: In this section new bounds L_{1E} and U_{1E} for the largest eigenvalue of $\boldsymbol{R}(\boldsymbol{Y}_k)$ in (24) are derived for the case when the error matrix is nonzero. The same method used in Section IV-B3 is applied, though with $\boldsymbol{A} = \sigma_x^2\boldsymbol{R}(\boldsymbol{X}_k) + \sigma_w^2\boldsymbol{R}(\boldsymbol{W}_k)$ and $\boldsymbol{B} = \boldsymbol{E}_k$. Using (29) and the upper bounds given in (35) and (37) the new upper bound can be written as

$$U_{1E} = U_1 + 2\sigma_x\sigma_w\sqrt{N}. \tag{40}$$

Similarly, using (30) and the lower bounds given in (35) and (39) the new lower bound can be shown to be

$$L_{1E} = L_1 - 2\sigma_x\sigma_w\sqrt{N}. \tag{41}$$

Figure 5 shows an example of the temporal variation of $\lambda_{Y,1}$ with the bounds from (37), (39), (40) and (41) for $\sigma_x^2 = \sigma_w^2 = 1$ and $N = 64$. The bounds U_1 and L_1 are exceeded in the figure since they neglect the error matrix.

V. Detection techniques

The detection of an unknown DSSS signal can be cast as a binary hypothesis testing problem

$$\begin{aligned} \mathcal{H}_0: \quad \boldsymbol{y}(nT_c) &= \sigma_w\boldsymbol{w}(nT_c) \\ \mathcal{H}_1: \quad \boldsymbol{y}(nT_c) &= \sigma_x\boldsymbol{x}(nT_c) + \sigma_w\boldsymbol{w}(nT_c) \end{aligned}$$

using the intercepted signal of (3) with the unknown deterministic signal $\boldsymbol{x}(nT_c) = \boldsymbol{d}(nT_c)\boldsymbol{c}(nT_c)$. $\mathcal{H}_0$ signifies the signal absent (noise-only) case and $\mathcal{H}_1$ the signal present case. The task of the detection receiver is to decide whether the signal of interest is present or not, based on a detection threshold derived from a test statistic under the $\mathcal{H}_0$ hypothesis.

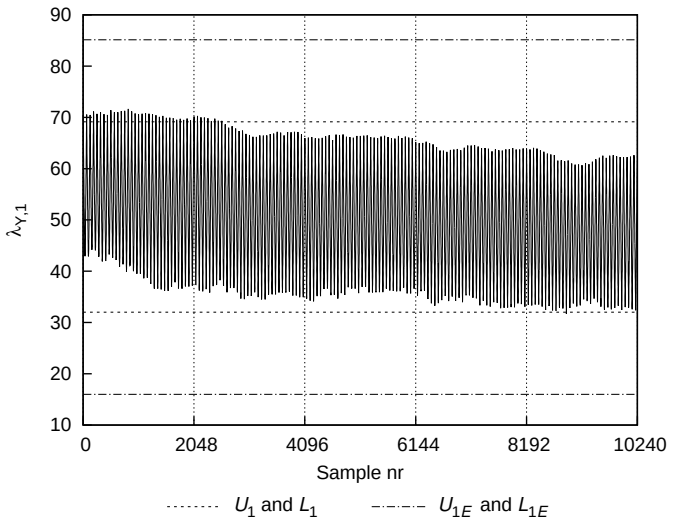

Fig. 5. Example temporal representation and bounds of $\lambda_{Y,1}$ for $\sigma_x^2 = \sigma_w^2 = 1$ and $N = 64$.

This section considers three techniques that can be used to detect DSSS signals. The techniques are classic ED and two new detection techniques based on eigen analysis presented in Sections III and IV. For ED the theoretical false alarm probability P_{FA} and detection probability P_D are derived in terms of the threshold. For the other two techniques, P_{FA} is derived in terms of the threshold and P_D is then determined using computer simulation with the results presented in Section VII.

A. Energy detection

Using the generalised likelihood ratio test, it can be shown that hypothesis $\mathcal{H}_1$ should be chosen if [7]

$$T(\boldsymbol{y}) = \sum_{n=1}^{V} \left[\boldsymbol{y}(nT_c)\right]^2 > \zeta \tag{42}$$

with $T(\cdot)$ signifying the test statistic function calculated over V samples and ζ the detection threshold which can be calculated from the required P_{FA} according to the Neyman-Pearson (NP) criteria. Clearly, (42) signifies ED. Assuming perfect knowledge of the unknown signal, a performance upper bound of the NP detector can be determined [7]. Assuming the signal of interest is BPSK with $\boldsymbol{x}(nT_c) = \pm 1$, the hypothesis test can be stated as

$$\begin{aligned} \mathcal{H}_0: \quad T(\boldsymbol{y}) &= \sum_{n=1}^{N} \left[\sigma_w \boldsymbol{w}(nT_c)\right]^2 \\ \mathcal{H}_1: \quad T(\boldsymbol{y}) &= \sum_{n=1}^{N} \left[\pm\sigma_x + \sigma_w \boldsymbol{w}(nT_c)\right]^2 . \end{aligned}$$

It can then be shown that

$$\begin{aligned} \mathcal{H}_0: \quad \frac{T(\boldsymbol{y})}{\sigma_w^2} &\sim \mathcal{X}_N^2 \\ \mathcal{H}_1: \quad \frac{T(\boldsymbol{y})}{\sigma_w^2} &\sim \mathcal{X}_N'^2(p_{nc}) \end{aligned}$$

with $\mathcal{X}_N^2$ the central and $\mathcal{X}_N'^2$ the non-central Chi-square distributions with noncentrality parameter

$$p_{nc} = \frac{N\sigma_x^2}{\sigma_w^2} = N \times \text{SNR}.$$

The false alarm probability can then be expressed as

$$\begin{aligned} P_{FA} &= p\left\{T(\boldsymbol{y}) > \zeta; \mathcal{H}_0\right\} \\ &= p\left\{\frac{T(\boldsymbol{y})}{\sigma_w^2} > \frac{\zeta}{\sigma_w^2}; \mathcal{H}_0\right\} \\ &= Q_{\mathcal{X}_N^2}(\zeta') \end{aligned} \tag{43}$$

with $Q_{\mathcal{X}_N^2}(\zeta')$ the right tail probability of $\mathcal{X}_N^2$ and the scaled threshold $\zeta' = \zeta/\sigma_w^2$. Likewise, the detection probability can be expressed as

$$P_D = Q_{\mathcal{X}_N'^2}(\zeta'). \tag{44}$$

B. Eigen detection technique 1

The first eigen detection algorithm is based on the feature extraction technique presented in Section III. The algorithm contains three phases. Firstly, the intercepted signal is segmented and stacked to form the detection matrix. Secondly, the principle component of the detection matrix is calculated and thirdly the detection matrix is cyclically shifted. The principle component is calculated for every cycle, such that the largest eigenvalue sequence $\lambda_{Y,1}$ is generated. A detection is declared if $\lambda_{Y,1}$ exceeds a given threshold ζ. This threshold can be calculated from the right tail probability

$$P_{FA} = Q_g(\zeta) = \int_{\zeta}^{\infty} \gamma(x)dx \tag{45}$$

with $\gamma(x)$ the PDF of $\lambda_{W,1}$ given in (22). The threshold is therefore

$$\zeta = Q_g^{-1}(P_{FA}). \tag{46}$$

The SNR limit at which perfect detection ($P_{FA} = 0$ and $P_D = 1$) is achieved can be calculated using the upper bound on $\lambda_{W,1}$ given in (23) and the lower bound on $\lambda_{Y,1}$ given in (41). For SNR values above this limit, $\lambda_{W,1}$ will always be less than $\lambda_{Y,1}$ such that

$$x_0 + 2\alpha\theta < L_1 - 2\sigma_x\sigma_w\sqrt{N} \tag{47}$$

with $L_1 = N\sigma_x^2/2$ from (39). The SNR limit can be calculated by solving the quadratic inequality for σ_x/σ_w that results when the parameter values x_0, α and θ from Section IV-A are substituted into (47). For example, perfect detection for $N = 64$ using technique 1 can be shown to be possible if SNR > -2.828 dB. For nonzero values of P_{FA}, $P_D = 1$ will be achieved below this SNR limit.

C. Eigen detection technique 2

As illustrated in Sections III and IV, $\lambda_{Y,1}$ exhibits a strong pattern with period N (or T_{sym}) as the detection matrix is cyclically shifted (if a DSSS signal is present). Detection could therefore be based on the frequency content $I(f_0)$ of $\lambda_{Y,1}$ at $f_0 = 1/T_{sym}$. Eigen detection technique 2 uses sinusoidal

detection to isolate $I(f_0)$ and declares a detection if a given threshold ζ is exceeded. The test statistic is therefore given by

$$T(\lambda_{Y,1}) = I(f_0) = \left[\frac{1}{\sqrt{V}}\sum_{n=1}^{V}\lambda_{Y,1}(nT_s)\cos(2\pi f_0 nT_s)\right]^2 + \left[\frac{1}{\sqrt{V}}\sum_{n=1}^{V}\lambda_{Y,1}(nT_s)\sin(2\pi f_0 nT_s)\right]^2 \quad (48)$$

which is the periodogram equation [7] for sinusoidal detection of unknown amplitude and phase over V samples. In order to calculate $I(f_0)$ for $\lambda_{Y,1}$ formed by the content of a single detection matrix, the number of samples should be $V = N^2$. V can however be chosen even longer, since the repetition pattern continues beyond N^2. Under $\mathcal{H}_0$, the PDF of $I(f_0)$ is related to the central Chi-square distribution with two degrees of freedom [7], since each term of the sum in (48) is normally distributed before squaring. The false alarm probability can therefore be given as

$$P_{FA} = Q_{\mathcal{X}_2^2}(\zeta') = \exp\left(-\frac{\zeta'}{2}\right) \quad (49)$$

similar to (43), from which the threshold can determined using

$$\zeta' = -2\,\ln(P_{FA}). \quad (50)$$

VI. Computational complexity

Computational complexity can be measured in terms of the total number of elementary arithmetic operations ($+$, $-$, $\times$, $\div$) required to execute an algorithm. The complexity of other operations can also be expressed in terms of the elementary operations. It will be assumed that the complexity of square rooting and division is the same as that of multiplication [24]. Likewise, addition and subtraction will be assumed equivalent. The complexity of an algorithm is typically dominated by the number of multiplications required, since multiplication is more complex than addition. This section considers the computational complexity of the three algorithms presented in Section V in terms of the number of arithmetic operations required to extract the test statistic from the intercepted data. Additional processing, such as memory allocation and movement of data values, is not taken into account. The equivalent number of multiplications and additions required for each algorithm are summarised in Table I and measured execution times are given Section VII-C.

A. Energy detection

ED is implemented in this paper using (42) with a fixed size window moving over the intercepted data. The window size V is equal to the size of the detection matrix N^2. The energy in a single window can therefore be calculated using N^2 multiplications and $N^2 - 1$ additions.

B. Eigen detection technique 1

The most computationally intensive step of the first eigen detection algorithm (described in Section V-B) is the calculation of the principle component, which involves calculating a SCM and its largest eigenvalue. The computational complexity of this step will subsequently be considered for a single cyclic shift of the detection matrix.

1) Calculation of the SCM: Equation (8) indicates that the SCM is calculated by performing matrix multiplication on two $N \times N$ matrices and scaling the resultant matrix by N. It might be more economical to rather scale the detection threshold value (see [12]) than to scale each of the N^2 elements of the resultant matrix (if the hardware platform allows large numbers). For the analysis presented here, it will be assumed that calculation of the SCM is equivalent to a single matrix multiplication operation. The matrix multiplication operation $\boldsymbol{F} = \boldsymbol{GH}$ can be implemented through the conventional approach [13] using

$$f_{ij} = \sum_{k=1}^{N} g_{ik}h_{kj} \quad (51)$$

where $[\cdot]_{ij}$ is the ij^{th} matrix element. Calculation of each element of $\boldsymbol{F}$ therefore requires N multiplications and $N-1$ additions. Since there are N^2 elements to be calculated, the overall matrix multiplication operation requires N^3 multiplications and $N^2(N-1)$ additions.

2) Calculation of the largest eigenvalue: Eigenvalues are usually approximated using iterative numerical methods, such as the power method [13], [25]. The power method is used to determine the dominant eigenvalue (or simply the largest eigenvalue, if the eigenvalues are nonnegative real) and associated eigenvector of the $N \times N$ matrix $\boldsymbol{F}$. The algorithm takes as input a nonzero column vector $\boldsymbol{v}_0$ (with unit Euclidean norm) which could be an approximation to the associated eigenvector or a random vector. If $\boldsymbol{F}$ is symmetric, the algorithm can be simplified and the largest eigenvalue λ_m and eigenvector $\boldsymbol{v}_m$ can then approximated using [25]

$$\boldsymbol{u}_m = \boldsymbol{F}\boldsymbol{v}_m \quad (52)$$

$$\lambda_m = \boldsymbol{v}_m^T\boldsymbol{u}_m \quad (53)$$

$$\boldsymbol{v}_{m+1} = \frac{\boldsymbol{u}_m}{||\boldsymbol{u}_m||_2} \quad (54)$$

$$\varepsilon = ||\boldsymbol{v}_{m+1} - \boldsymbol{v}_m||_2 \quad (55)$$

for each $m^{\text{th}}, m \geq 0$ iteration, with $||\cdot||_2$ signifying the Euclidean norm. The convergence of the algorithm depends on $\boldsymbol{F}$ and the choice of $\boldsymbol{v}_0$. Although bad choices of $\boldsymbol{v}_0$ may result in slow convergence or division by zero errors (the algorithm will then not converge and will need to be restarted with a new $\boldsymbol{v}_0$), the algorithm will converge for almost all initial guesses of $\boldsymbol{v}_0$ if $\boldsymbol{F}$ has a single dominant eigenvalue (see [26]). The algorithm should therefore check at each iteration whether $||\boldsymbol{u}_m||_2 = 0$. The number of iterations can be limited to a specified maximum or the algorithm can stop when the tolerance ε decreases below a predefined value. The computational complexity of the symmetric power method is considered below, assuming the algorithm will converge.

TABLE I
COMPARATIVE COMPUTATIONAL COMPLEXITIES OF THE THREE DETECTION ALGORITHMS.

Algorithm	Multiplications	Additions
ED	N^2	N^2-1
Tech 1	$N^3+M(N^2+4N+2)$	$N^3-N^2+M(N^2+3N-3)$
Tech 2	$2V+3$	$2V-1$

(52) is a matrix-vector multiplication which is the same as (51) with $j=1$. Since only N elements are calculated, (52) requires N^2 multiplications and $N(N-1)$ additions. (53) is a dot-product operation and requires N multiplications and $N-1$ additions. (54) requires N divisions and the calculation of the Euclidean norm, which requires N multiplications, $N-1$ additions and one square root calculation. Lastly, (55) requires N subtractions and again the calculation of an Euclidean norm. Assuming M iterations are required to reach a certain ε, calculation of the largest eigenvalue therefore requires the equivalent processing time of $M(N^2+4N+2)$ multiplications and $M(N^2+3N-3)$ additions.

3) Possible simplifications: A more efficient (though with reduced numerical stability) method to perform matrix multiplication is Strassen's algorithm [13], [27]. The algorithm recursively splits the matrices to be multiplied into smaller submatrices and performs matrix multiplication using less multiplications, but more additions than the conventional approach. The multiplicative cost of the Strassen algorithm is $O(N^{\log_2 7}) \approx O(N^{2.807})$, instead of $O(N^{\log_2 8}) = O(N^3)$ of the conventional approach.

An alternative method to approximate the largest eigenvalue is the trace method [28] using

$$\mathrm{tr}\left(\boldsymbol{F}^{\,r}\right) = \sum_{i=1}^{N} \lambda_i^r. \tag{56}$$

If $\lambda_1 >> \lambda_2$ it follows from (56) that $\mathrm{tr}\left(\boldsymbol{F}^{\,r}\right) \approx \lambda_1^r$ such that

$$\lambda_1 \approx \left[\mathrm{tr}\left(\boldsymbol{F}^{\,r}\right)\right]^{\frac{1}{r}}. \tag{57}$$

The larger the difference between the largest and other eigenvalues, the better the approximation. Computation of (57) requires $r-1$ matrix multiplications, $N-1$ additions to calculate the trace and the calculation of the r^{th} root of a real number. If $\boldsymbol{F}$ could have negative eigenvalues, r should be odd in order to retain the correct eigenvalue sign and the minimum value is then $r=3$. However, when $\boldsymbol{F}$ is positive-semidefinite (all eigenvalues are nonnegative real) the minimum value is $r=2$. Although the trace method will not produce accurate eigenvalues for the matrices considered in this paper, it can be used to produce a periodic eigenvalue sequence.

C. Eigen detection technique 2

Technique 2 calculates the frequency content of $\lambda_{Y,1}$ produced by technique 1. The complexity can be calculated by writing (48) as

$$T(\lambda_{Y,1}) = \frac{1}{V}\left[\left(\sum_{n=1}^{V}\lambda_{Y,1}(nT_s)f_{\cos}(nT_s)\right)^2 + \left(\sum_{n=1}^{V}\lambda_{Y,1}(nT_s)f_{\sin}(nT_s)\right)^2\right] \tag{58}$$

with $f_{\cos}$ and $f_{\sin}$ representing cosine and sine function values which can be calculated once and stored in memory. Each term within the square brackets of (58) requires $V+1$ multiplications and $V-1$ additions. The total complexity of (58) is therefore equivalent to $2V+3$ multiplications and $2V-1$ additions. To calculate the total processing time to produce a single value of $T(\lambda_{Y,1})$, the time required to produce the V samples of $\lambda_{Y,1}$ used in (58) should also be included.

VII. SIMULATION STUDY AND RESULTS

The performances of the three detection techniques were evaluated through Monte Carlo computer simulation with the target communication system a baseband BPSK DSSS system employing a length $N=64$ binary Walsh spreading code (taking row 32 of the Walsh matrix as code sequence). The intercept receiver used 1 sample per code chip such that $T_s = T_c$ to perform detection. The number of samples used to calculate a single test statistic value (for a single cyclic shift) for each detection technique was $N_s = N^2 = 64^2 = 4096$ corresponding to the size of the detection matrix. Since eigen technique 2 calculates the frequency content of the eigenvalue sequence and is not confined to the size of the detection matrix, the value $10N^2 = 40960$ was also considered for this technique. This section presents the simulated false alarm and detection performance results where 10^6 data bits were considered per simulation run. A single simulation run consisted of calculating the probability of detection for a given SNR value. Measured average execution times for each technique are also presented.

A. Calculation of false alarm rates

The false alarm performance of each technique was measured by calculating the theoretical threshold ζ from set values of P_{FA} using the equations in Section V. The false alarm or detection probability for the noise-only scenario was then obtained by setting $\sigma_x = 0$ and $\sigma_w = 1$ in (3). The results are given in Table II. To obtain improved accuracies of these values or to measure even lower probabilities, larger values of N_s would be required. The measured values in Table II however correspond closely to the set values, confirming that the threshold equations in Section V are correct.

TABLE II
MEASURED FALSE ALARM PROBABILITY VALUES.

Set P_{FA}	ED	Tech 1	Tech 2
0.001	0.0010205	0.0012686	0.0009245
0.003	0.0030093	0.0034905	0.0027469
0.005	0.0050614	0.0056225	0.0046470
0.010	0.0101522	0.0107803	0.0099211
0.030	0.0302207	0.0307656	0.0309257
0.050	0.0504181	0.0505104	0.0514241
0.100	0.1007815	0.0997421	0.1010004
0.300	0.3005873	0.2995871	0.2995768
0.500	0.5012642	0.5045618	0.4978770

B. Probability of detection performance

Using the theoretical threshold values calculated from the set values of P_{FA} and setting $\sigma_w = 1$ in (3) and σ_x according to (4) for a given SNR value, simulated values for P_D were obtained. The simulated detection performances for $P_{FA} = 0.1$ and $P_{FA} = 10^{-6}$ are shown respectively in Figures 6 and 7. At $P_{FA} = 10^{-6}$ technique 1 exhibits a maximum performance gain of approximately 3 dB over ED. Technique 2 exhibits additional gains over technique 1 of 1.5 dB for $V = N^2$ and 4 dB for $V = 10N^2$.

Figure 7 shows that for $P_{FA} = 10^{-6}$, technique 1 achieves $P_D = 1$ at $\mathrm{SNR} = -10$ dB. The SNR value at which $P_D = 1$ is reached increases with decreasing P_{FA}. Technique 1's theoretic limit for perfect detection (see Section V-B) however predicts the value at which $P_D = 1$ is reached will not increase beyond $\mathrm{SNR} = -2.828$ dB.

The receiver operating curves (ROCs), displaying the P_D vs. P_{FA} performance, for $\mathrm{SNR} = -14$ dB and the reference 45° line are shown in Figure 8. For values of P_{FA} approaching one, the three techniques have the same detection performances, though for values of P_{FA} approaching zero both eigen detection techniques are superior to ED. At $\mathrm{SNR} = -14$ dB, technique 2 ($V = 40960$) exhibits perfect detection. As the SNR value decreases, the ROC curves moves closer to the 45° reference line.

C. Evaluation of execution time

Although the number of arithmetic operations required to execute an algorithm (as derived in Section VI) predicts execution time, several other factors should also be considered. Two most important factors determining execution speed are hardware platform specifications (processing speed, memory size, etc.) and the efficiency of the implementation (how well the code is written to exploit the hardware).

The measured average execution times matching Table I are given in Table III for different code lengths N. The three techniques were implemented using ANSI *C* on a computer platform with an Intel Core 2 Duo T9600 (2.80 GHz) processor. The average execution time was measured by counting the number of processing cycles required by the section of *C* code that calculates the test statistic. The implementation of technique 1 was also enhanced using basic linear algebra sub-

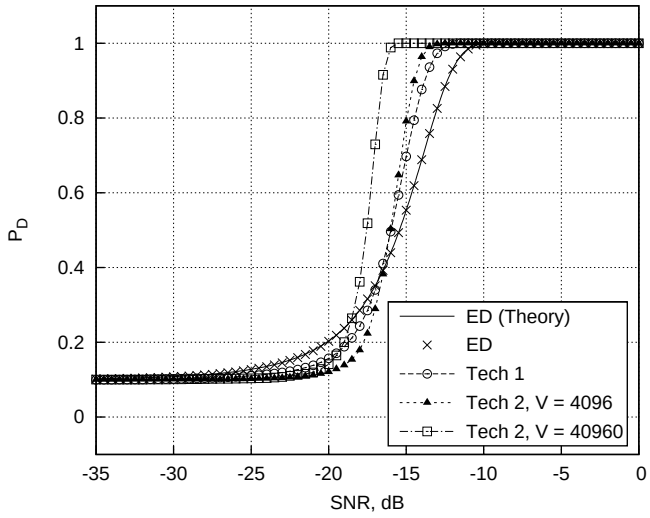

Fig. 6. Simulated detection performance for $P_{FA} = 0.1$.

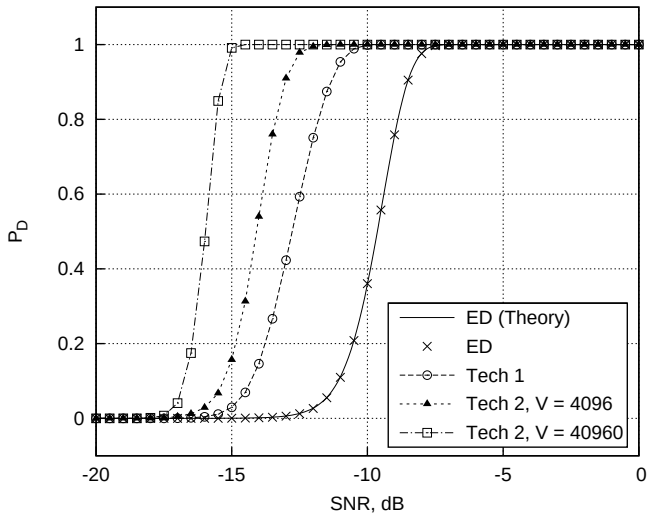

Fig. 7. Simulated detection performance for $P_{FA} = 10^{-6}$.

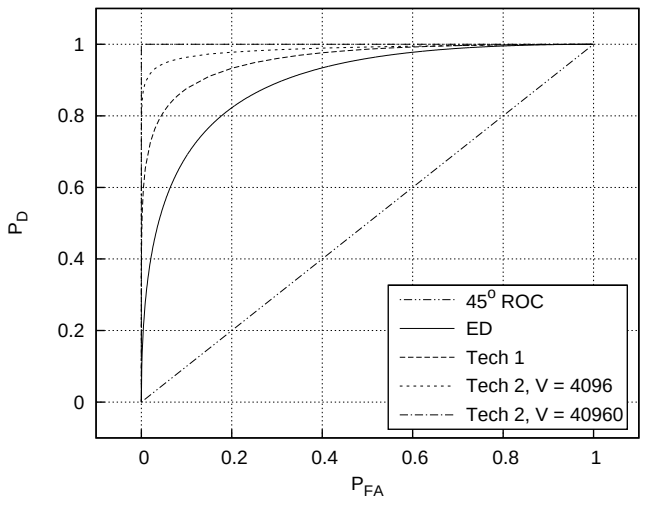

Fig. 8. Simulated receiver operating curves for SNR = -14 dB.

TABLE III
AVERAGE EXECUTION TIME IN SECONDS OF THE DETECTION ALGORITHMS FOR DIFFERENT VALUES OF N.

Algorithm	$N = 32$	$N = 64$	$N = 96$	$N = 128$
ED (*C*)	3.2928×10^{-6}	1.2870×10^{-5}	2.9118×10^{-5}	5.1695×10^{-5}
Tech 1 (*C*, -5 dB)	2.4120×10^{-4}	1.4825×10^{-3}	4.9252×10^{-3}	1.2397×10^{-2}
Tech 1 (GSL, -5 dB)	7.7575×10^{-5}	3.5204×10^{-4}	1.1936×10^{-3}	2.5524×10^{-3}
Tech 1 (*C*, -25 dB)	4.8001×10^{-4}	2.8274×10^{-3}	1.0530×10^{-2}	2.5837×10^{-2}
Tech 1 (GSL, -25 dB)	1.8533×10^{-4}	8.1181×10^{-4}	3.0881×10^{-3}	6.5832×10^{-3}
Tech 2 (*C*, $V = N^2$)	5.7688×10^{-6}	2.3089×10^{-5}	5.2298×10^{-5}	9.2508×10^{-5}
Tech 2 (*C*, $V = 10N^2$)	5.7705×10^{-5}	2.3179×10^{-4}	5.2073×10^{-4}	9.2447×10^{-4}

programs (BLAS) [29] through the *C* Gnu Scientific Library (GSL) [30].

For ED, the complexity only depends on N and the values in Table III clearly indicates that the execution time is related to N^2 as predicted in Table I. The complexity of technique 1 depends both on N and the number of iterations M required by the symmetric power method. M is a function of SNR and the tolerance value ε; the power method converges slower for smaller values of both SNR and ε. The detection performance results presented in this paper can be obtained using $\varepsilon = 10^{-4}$ (smaller values do not improve performance) which is reached on average after $M = [11, 70, 111]$ iterations respectively for $\mathrm{SNR} = [-5, -15, -25]$ dB.

Table III contains execution time results for technique 1 for $\mathrm{SNR} = -5$ and -25 dB. The results of both the *C* and *C* with GSL implementations are shown. All four technique 1 cases indicate a growth in execution time greater than N^2. However, using GSL reduces the execution times and growth rates. Lastly, the execution times of technique 2 are strongly related to N^2 in each case (as predicted in Table I). By increasing the window length N^2 by a factor 10, the execution times increase by the same factor.

Comparing the different techniques using Tables I and III, it is clear that ED is the least complex. Although technique 2 is faster than technique 1, technique 2 needs the output sequence produced by technique 1.

VIII. CONCLUSION

This paper considered the detection of weak DSSS signals using PCA. Two new semi-blind detection techniques with superior performance to classic ED were presented. If the carrier frequency is known, the techniques only require the sequence length of the spreading code to construct a detection matrix which forms the basis of detection. It was shown that a DSSS signal can be detected using a function of the largest eigenvalue of the shifted detection matrix as test statistic. The performance improvement is due to the large difference between the largest eigenvalues of the detection matrix under the $\mathcal{H}_0$ and $\mathcal{H}_1$ hypotheses even at low SNR values. The computational complexity of each algorithm was also evaluated. Although this paper focussed on real signals, the techniques can also be applied to complex signals since the eigenvalues of the SCM of a complex detection matrix will also be real.

IX. ACKNOWLEDGEMENT

This work was supported by the Armaments Corporation of South Africa (Armscor) under contract no. KT521896. The authors would like to thank the anonymous reviewers for their valuable inputs.

REFERENCES

1 Dillard, R., and Dillard, G.M.: 'Detectability of spread-spectrum signals' (Artech House, Norwood, MA, USA, 1989, 1st edn.)
2 Adams, E.R., Gouda, M., and Hill, P.C.J.: 'Statistical techniques for blind detection & discrimination of m-sequence codes in DS/SS systems'. Proc. Int. Symp. Spread Spectrum Techniques and Applications, Sun City, South Africa, September 1998, pp. 853–857
3 Burel, G., Bouder, C., and Berder, O.: 'Detection of direct sequence spread spectrum transmissions without prior knowledge'. Proc. IEEE-Globecom, San Antonio, TX, USA, November 2001, pp. 236–239
4 Zhan, Y., Cao, Z., and Lu, J.: 'Spread-spectrum sequence estimation for DSSS signal in non-cooperative communication systems', IEE Proc. Commun., 2005, 152, (4), pp. 476–480
5 Bouder, C., Azou, S., and Burel, G.: 'Performance analysis of a spreading sequence estimator for spread spectrum transmissions', Elsevier J. Franklin Inst., 2004, 341, (7), pp. 595–614
6 Bouder, C., and Burel, G.: 'Spread spectrum codes identification by neural networks', in Mastorakis, N. (Ed.): 'Systems and Control: Theory and Applications' (WSES Press, 2000), pp. 257–262
7 Kay, S.M.: 'Fundamentals of statistical signal processing: detection theory' (Prentice Hall, Upper Saddle River, NJ, USA, 2011, 1st edn.)
8 Proakis, J.G., and Salehi, M.: 'Digital Communications' (McGraw-Hill, 2007, 5th edn.)
9 Olivier, K., Cilliers, J.E., and Du Plessis, M.: 'Design and performance of wideband DRFM for radar test and evaluation', Electronics Lett., 2011, 47, (14), pp. 824–825
10 Bejan, A.: 'Largest eigenvalues and sample covariance matrices'. MSc dissertation, University of Warwick, UK, 2005
11 Johnstone, I.M.: 'On the distribution of the largest eigenvalue in principal component analysis', Ann. Statist., 2001, 29, (2), pp. 295–327
12 Vlok, J.D., and Olivier, J.C.: 'Analytic approximation to the largest eigenvalue distribution of a white Wishart matrix', IET Commun., 2012, 6, (12), pp. 1804–1811
13 Golub, G.H., and Van Loan, C.F.: 'Matrix computations' (John Hopkins University Press, Baltimore, MD, USA, 1996, 3rd edn.)
14 Wei, W., and Tirkkonen, O.: 'Analysis of scaled largest eigenvalue based detection for spectrum sensing'. Proc. IEEE Int. Conf. Comms., Kyoto, Japan, June 2011, pp. 295–327
15 Everson, R., and Roberts, S.: 'Inferring the eigenvalues of covariance matrices from limited, noisy data', IEEE Trans. Signal Process., 2000, 48, (7), pp. 2083–2091
16 Horn, R.A., and Johnson, C.R.: 'Matrix analysis' (Cambridge University Press, Cambridge, UK, 2012, 2nd edn.)
17 Tao, T.: 'Topics in random matrix theory (Graduate studies in mathematics)' (American Mathematical Society, Rhode Island, USA, 2012)
18 Li, C.K., and Poon, Y.T.: 'Sum of Hermitian matrices with given eigenvalues: inertia, rank, and multiple eigenvalues', Canad. J. Math., 2010, 62, (1), pp. 109–132
19 Zhan, X.: 'Extremal eigenvalues of real symmetric matrices with entries in an interval', SIAM J. Matrix Anal. Appl., 2006, 27, (3), pp. 851–860

20 Wu, J.: 'Upper (lower) bounds of the eigenvalues, spread and the open problems for the real symmetric interval matrices', Math. Meth. Appl. Sci., 2012, in print, DOI:10.1002/mma.2601

21 Wigner, E.P.: 'On the distribution of the roots of certain symmetric matrices', Ann. Math, 1958, 67, (2), pp. 325–327

22 Dean, S.D., Majumdar, S.N.: 'Extreme value statistics of eigenvalues of Gaussian random matrices', Phys. Rev. E, 2008, 77, (4), pp. 041108-1–041108-12

23 Silverstein, J.W.: 'Eigenvalues and eigenvectors of large dimensional sample covariance matrices', Contemp. Math., 1986, 50, pp. 153–159

24 Muller, J-M.: 'Elementary functions: algorithms and implementation' (Birkhäuser, Boston, USA, 2006, 2nd edn.)

25 Burden, R.L., and Faires, J.D.: 'Numerical Analysis' (Cengage Learning, MA, USA, 2011, 9th edn.)

26 Smale, S.: 'Complexity Theory and Numerical Analysis', Acta Numer., 1997, 6, pp. 523–551

27 Strassen, V.: 'Gaussian elimination is not optimal', Numer. Math., 1969, 13, pp. 354–356

28 Gonzalez, E.A.: 'Determination of the dominant eigenvalue using the trace method', IEEE MEEM, 2006, 1, (1), pp. 1–2

29 http://www.netlib.org/blas, accessed July 2012

30 http://www.gnu.org/software/gsl, accessed July 2012